Nanoscale

Accepted Manuscript

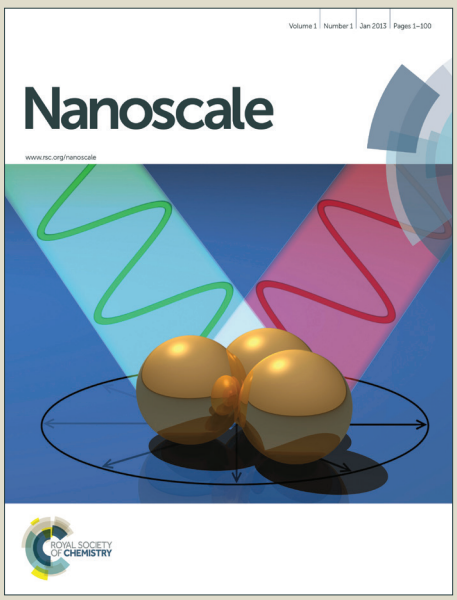

ROYAL SOCIETY OF CHEMISTRY

www.rsc.org/nanoscale

Nanoscale

RSCPublishing

ARTICLE

Asymmetric Half-Cone/Nanohole Array Films with Structural and Directional Reshaping of Extraordinary Optical Transmission

Cite this: DOI: 10.1039/xoxxoooooox

Bin Ai,[a] Limin Wang,[a] Helmuth Möhwald,[b] Ye Yu,[a] and Gang Zhang*[a]

Received ooth January 2012,
Accepted ooth January 2012

DOI: 10.1039/xoxxoooooox

www.rsc.org/

Structured films with periodic arrays of nanoholes covered by half-cone shells are fabricated via a simple and efficient colloidal lithography method. The designed films show strong polarization dependence in optical transmission. By decreasing the height of half-cone shells the peak shifts and this shift varies strongly for different orthogonal polarization. Furthermore, the three-dimensional (3D) asymmetric arrays exhibit a pronounced increase of the transmission intensity by changing the direction of the incident light from the half-cone shell (shelter) side to the empty side. Special surface plasmon resonances excited by the unique 3D asymmetric structure are responsible for these novel properties, and the experimental results are in good agreement with numerical simulations. The nanostructured films in this work will be useful for metallic nanophotonic elements in many applications, including surface plasmon enhanced optical sensing and ultrafast optical switching, as well as versatile substrates for surface enhanced Raman spectroscopy, anisotropic wettability and other potential uses.

1 Introduction

The discovery of the extraordinary optical transmission (EOT) in arrays of subwavelength holes,[1] drilled into optically thick metal films, has attracted a great deal of attention, due both to its fundamental character and potential applications in optical filters,[2] imaging,[3] photonic circuits,[4] fluorescence,[5] sensors,[6] surface enhanced Raman spectroscopy (SERS),[7] among others. Further research showed that surface electromagnetic modes play a key role in the emergence of the resonant transmission.[1,8,9] Moreover, the influence of the material,[10,11] hole diameter,[12-14] shape,[15,16] polarization[17-19] and finite-size[20-23] of the nanohole array were investigated to further clarify the physical mechanism as well as the enhanced optical performance. For more optimized applications, nanohole arrays have been much developed in impressive extensive work. For example, quasi-3D plasmonic crystals that consist of multilayered nanostructures[24-28] and mushroom like composite metallodielectric nanostructure[29] were fabricated with improved characteristics for surface plasmon resonance (SPR). By purposefully applying the colloidal lithography technique, opening nanodome arrays,[30] nanovolcano arrays[31] and hollow nanocone arrays[32] were prepared, which are well suited for high sensitivity applications, monochromatic color displays and novel optics. In particular, the 3D nanohole arrays prove to have unique advantages relative to 2D ones and may represent a qualitative advancement of nanohole arrays.[33] SPR can be greatly enhanced by these non-planar structures.

Up to now the majority of work has been focused on the films with symmetrical 3D nanohole arrays, 3D ones with in-plane asymmetry have been scarcely explored. Till very recently, 3D crescent-like holes arrays were fabricated and investigated for the fundamental performance of SPR, which was the first report about EOT in a non-planar asymmetric structure.[34] Fabrication of other 3D asymmetric nanohole arrays with more peculiar properties, exploring the relation between the unique properties and nanopatterned surfaces and making use of these is still in progress. Novel types of 3D asymmetric nanohole arrays with well-designed structures are strongly demanded for potential advanced optical properties. The generation and development of desirable nanostructures profit from recent advances in nanofabrication techniques. While conventional lithography techniques such as electron beam[35] and focused ion beam lithography[36,37] are capable of precise control over the size, shape, and spacing of metallic nanostructures, more recent research has focused on unconventional lithographic techniques that are capable of patterning large areas in parallel at low cost. In particular, colloidal lithography has been widely exploited in the fabrication of surface plasmonic structures, possessing advantages of lower cost, higher throughput, greater flexibility and easier implementation. By using two-dimensional colloidal crystals as templates, metal crescents, discs, holes, and split-ring resonators have been prepared after various metal evaporation processes and reactive-ion etching (RIE) procedures.[38-42]

Here, based on our previous work on colloidal lithography (CL),[43-45] we present a method to prepare novel films with 3D asymmetric nanohole arrays covered by the half-cone shells (shelters). The asymmetric half-cone/nanohole array films are capable of reshaping the optical transmission for differently polarized light, structural parameters and incidence angle. A novel spectral signature of nanohole arrays is presented and further shows large differences for orthogonal polarization of

the incident light. Besides, different spectral dependences on structural parameters are also shown. Finite-difference time-domain (FDTD) simulations reveal that different SPR modes and excitation locations can account for these novel optical properties. Furthermore while the angle-dependent transmissions of the planar nanohole as well as the full-cone arrays are both symmetric, the asymmetric half-cone/nanohole array films show an advanced property of asymmetric angle-dependent transmission with intensity increasing with changing the direction of the incident light from the shelter (half-cone shells) side to the empty side. The nanostructures thus have one more degree of asymmetry and hence of freedom for manipulation compared to the previous ones. This novel finding is believed to offer great potential for novel sensors and optics. In addition one obtains more detailed data to arrive at a more quantitative understanding.

2 Experimental

2.1 Materials

In all experiments the deionized water was ultrapure (18.2 MΩ•cm) from a Millipore water purification system. The glass slides used as substrates were cleaned in an O_2 plasma cleaner for 2 min to create a hydrophilic surface. 700-nm PS spheres were obtained from Wuhan Tech Co., Ltd. Photoresist (BP212-37 positive photoresist) was purchased from Kempur (Beijing) Microelectronics, Inc. The silver (99.9%) powder for vapor deposition was purchased from Sinopharm Chemical Reagent Co. Ltd. Ethanol was purchased from Beijing Chemical Works, and used as-received.

2.2 Fabrication of Asymmetric Half-cone/Nanohole Array Films

Photoresist was spin-coated onto the glass substrate and cured at 88°C for 2 h. Next the PS sphere (700 nm) monolayers were prepared onto the as-prepared substrate by the interface method.[46] Oxygen reactive ion etching (RIE), performed on a Plasmalab Oxford 80 Plus system (ICP 65) system (Oxford Instrument Co., UK), was applied for 240, 270, 300 and 330 s, eliminating the PS spheres and generating cones with heights of 600, 500, 400 and 300 nm. The RIE procedure was operated at a pressure of 10 mTorr, a flow rate of 50 sccm, a radio-frequency (RF) power of 100 W and an inductively coupled plasma (ICP) power of 200 W. After that the samples were mounted in a thermal evaporator to deposit 100-nm Ag with an angle of 40°. Finally the photoresist was washed away by ethanol. After these procedures, the asymmetric half-cone/nanohole array was formed.

2.3 FDTD Simulations

A commercial software package (FDTD Solutions v8.6.3, Lumerical Solutions Inc.) was used to perform simulations of electromagnetic fields with the same structural parameters as extracted from the actual fabricated samples. The structure was excited by a normally incident, unit magnitude plane wave propagating in the z direction with an electric field polarization along the x-axis. A rectangular unit cell consisting of one hole in the center and four quartering holes at the four corners was used with periodic boundary conditions in two dimensions to simulate an infinite array of periodic asymmetric half-cone/nanoholes, and perfectly matched layer (PML) boundary conditions were used on the top and bottom surfaces of the simulation domain, respectively. The auto non-uniform mesh was chosen in the entire simulation domain for higher numerical accuracy, while the time step was small enough to satisfy the Courant stability condition. The mesh refinement is the conformal variant 2. Monitors of frequency-domain field profile and frequency-domain field and power were placed to calculate the distribution of SP energy and the transmission spectra in the continuous wave (CW) normalization state. The magnitude of the incident electric fields was taken to be unity, and the enhancement of electromagnetic fields evaluated. The optical parameters of Ag and SiO_2 were taken from Palik's handbook. Besides, the Bloch boundary conditions are used on the surfaces which are perpendicular to the x-y plane in the simulations of the angle-dependent transmission.

2.4 Characterization

Scanning electron microscopy (SEM) images were taken with a JEOL JSM 6700F field emission scanning electron microscope with a primary electron energy of 3 kV, and the samples were sputtered with a layer of Pt (ca. 2 nm thick) prior to imaging to improve conductivity. A Shimadzu 3600 UV-vis-NIR spectrophotometer with a polarization apparatus was used to measure the transmission spectra.

3 Results and Discussion

3.1 Fabrication of Asymmetric Half-cone/Nanohole Array Films

Highly ordered asymmetric half-cone/nanohole arrays were fabricated based on a well-developed colloid lithography[45] and shadow metal deposition, as shown in Figure 1A. In brief, ordered polystyrene (PS) sphere monolayers were first prepared on a glass substrate coated by a photoresin film. After that RIE with increasing duration was carried out to completely etch away the microspheres and construct the photoresin film into a periodic cone array. Next, a shadow deposition method with an angle of 40° was employed to deposit a 100-nm layer of silver on one half of the photoresin nanocones and inter-cone surface.

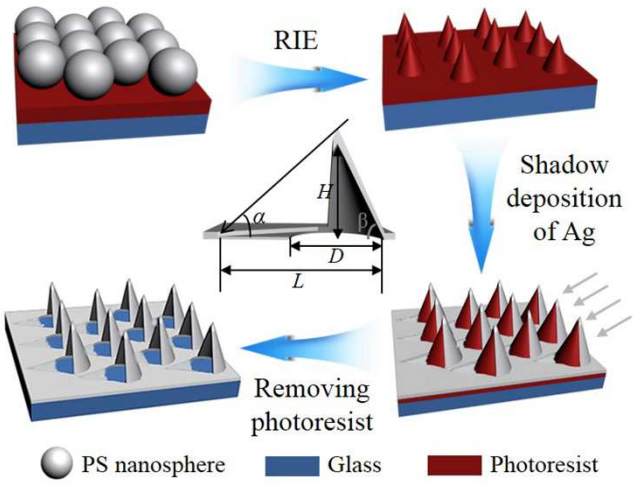

Figure 1. Outline of the process for fabricating asymmetric half-cone/nanohole arrays. The central schematic shows the cross section of a single asymmetric half-cone/nanohole and the main structural parameters.

A flat silver film with this thickness is optically nontransparent. The as-prepared sample was then immersed in ethanol to remove the photoresin. Finally, asymmetric half-cone/nanohole arrays were formed. In addition because of the scatter of the Ag vapor in the deposition process and the gradually weaker blocking effect from the bottom to the tip due to the conic structure, the area of the deposited Ag is a little larger than the area of the half-cones and some Ag also appears in the shadow. The central schematic shows a cross sectional view of a unit cell marked by the main structural parameters. In the fabrication process the period (P), height (H), thickness (T) and length (L) can be well controlled by the diameter of the PS spheres, etching parameters, deposition duration (rate) and incidence angle (α), respectively. The method is versatile, inexpensive and capable of patterning large areas in parallel at low cost and can be applied with only little sophisticated equipment, yet with good control of the main structural parameters.

By varying the etching duration, asymmetric half-cone/nanohole arrays with different heights and hole diameters are fabricated, as shown in Figure 2. The main parameters are shown in Table 1. When RIE processes are carried out, PS microsphere mask and photoresin film are both etched, yet with different etching rates. After the shadow deposition procedure and removal of the photoresin nanocones, asymmetric half-cone/nanohole arrays with designed parameters are formed and stably attached on the substrates because of the adhesive power between the Ag film and the glass substrate. However, the films also can be free-standing and further transferred to other substrates.[29] By prolonging the etching duration, the height

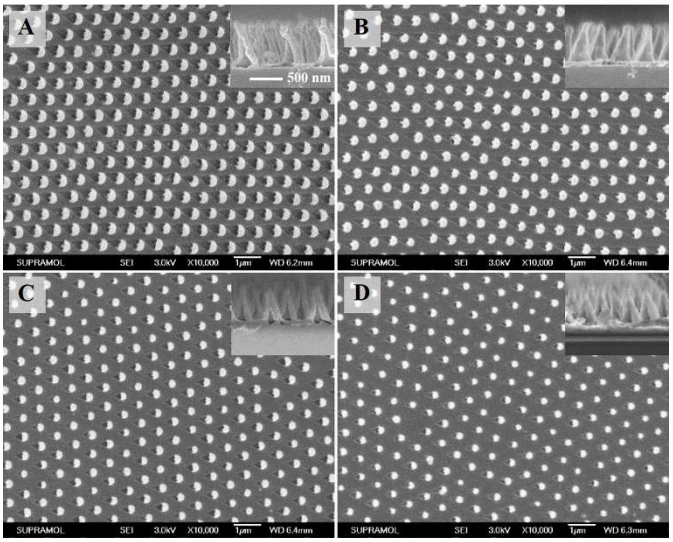

Figure 2. SEM images of the asymmetric half-cone/nanohole arrays with decreasing heights and hole diameters from (A) to (D). The structural parameters are shown in Table 1. The inset images show the cross sectional view of the corresponding asymmetric half-cone/nanohole arrays. The scale bar applies to all the inset images.

changes a lot from 600 nm to 300 nm, and the diameter changes much more slightly from 400 nm to 300 nm. Besides, the angle β changes a little, which indicates that the nanostructure is nearly scaled down. More SEM images are presented in Figure 3 for clarity of the nanostructures. The arrays in our work can be fabricated uniformly over a large area with dozens of micrometers as shown in Figure 3A, also unavoidably with some defects due to the characteristics of the CL technique.[44] The surface area is essentially identical within experimental error. Figure 3(B-E) show SEM images taken from different views indicated by the arrows in the inset schematic of Figure 3A. The area of the Ag shells is a little larger than the area of the half-cones and some Ag (always in the form of nanoparticles, not a continuous film) emerges in the shadow which ought to be empty (Figure S1). These features result from the scatter of the Ag vapor in the deposition process and the gradually weaker blocking effect from the bottom to the tip because of the conic structure. In particular, the shells are approximated as half cones for convenience. With emphasis on the novelty of the basic configuration, we demonstrate that the cone shells are fabricated on the nanohole arrays and cover half of the holes leading to the 3D asymmetric feature. Because of these structural characteristics, the nanostructures are called asymmetric half-cone/nanohole arrays.

Table 1. Structural parameters of asymmetric half-cone/nanohole arrays fabricated in this work.

Sample[a)]	Etching duration [s]	Height [H, nm] [b)]	Hole diameter [D, nm] [b)]	Length [L, nm] [b)]	Angle [β, °]
A	240	600	400	700	72
B	270	500	350	610	71
C	300	400	320	460	68
D	330	300	300	350	63

[a)] The samples correspond to those in Figure 2; [b)] the structural parameters correspond to those described in Figure 1 and have an error of 10 nm.

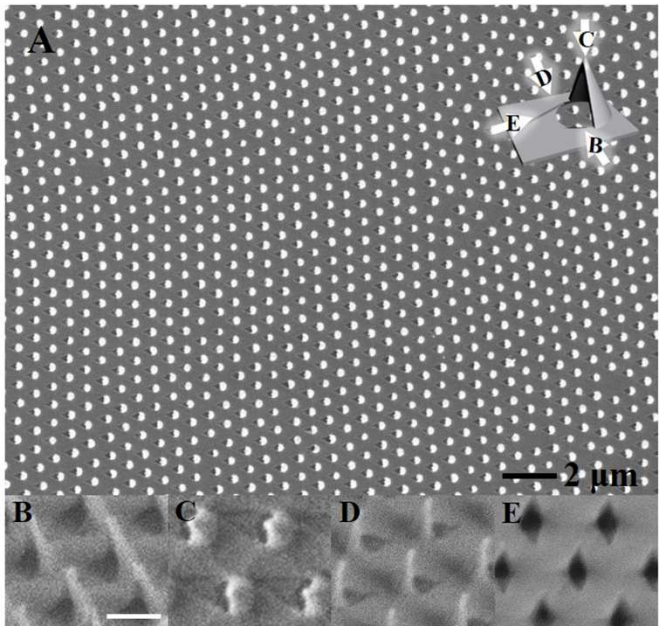

Figure 3. (A) SEM image of the asymmetric half-cone/nanohole array with 400-nm tip height over a large area. The image is taken from the top. SEM images of asymmetric half-cone/nanohole arrays with tip heights of (B) 600 nm, (C) 500 nm, (D) 400 nm and (E) 300 nm. The image in (C) is taken from a top view. The images in (B, D and E) are taken from a 45° tilting view. The orientations of the images are indicated in the inset image in (A). The scale bar in (B) corresponds to 500 nm and also applies to the images (C-E).

3.2 Strong Polarization of the Optical Transmission

To characterize the optical properties of asymmetric half-cone/nanohole arrays, we measured the zero-order transmission for normal incidence with polarization along the two main orthogonal axes. The transmission spectra were measured with the asymmetric half-cone/nanohole arrays attached on the glass substrates, which is also the condition in all following measurements. Figure 4A shows the results for the electric field along the y axis as shown in the inset image. Two transmission peaks emerge at 1257 and 2340 nm, and the transmission intensity of the latter one is much larger than that of the former one. The transmission spectrum measured for polarization along the x axis is shown in Figure 4B. There are two peaks at 1333 and 2070 nm with less different intensity than those in Figure 4A. These results demonstrate the strong polarization dependence of the spectra. In order to understand this, transmission spectra of the asymmetric half-cone/nanohole arrays have been simulated via the FDTD method. The respectively. At peak positions indicated by the blue, green and yellow dots, the electric field is concentrated on the Ag/glass interface and strongly localized at the hole edge (Figure 4C); trapped within the sharp tip (Figure 4D); excited at the tip and Ag/glass interface(Figure 4E). These distributions of SP energy are determined by the 3D asymmetric nanostructure and further demonstrate the elements dominating the transmission peaks. When the electric field is along the y (short) axis, the distance between the hole edge in a unit cell is small (400 nm). This would enhance the interaction of the hole edge and then enable SP energy to be localized on the Ag/glass interface and hole edge. Therefore, the broad peak at 2340 nm in Figure 4A is caused by the localized SPR (LSPR).

When the electric field is oriented along the much longer axis x of periodicity (700 nm), the interaction between the hole edges is much weaker. Therefore, the maximum of the electric field shifts to the tip. The enhanced SP energy is mainly caused by the conical structure rather than the periodicity. This indicates that the LSPR excited by the tip is the element determining the enhanced transmission at 2070 nm in Figure

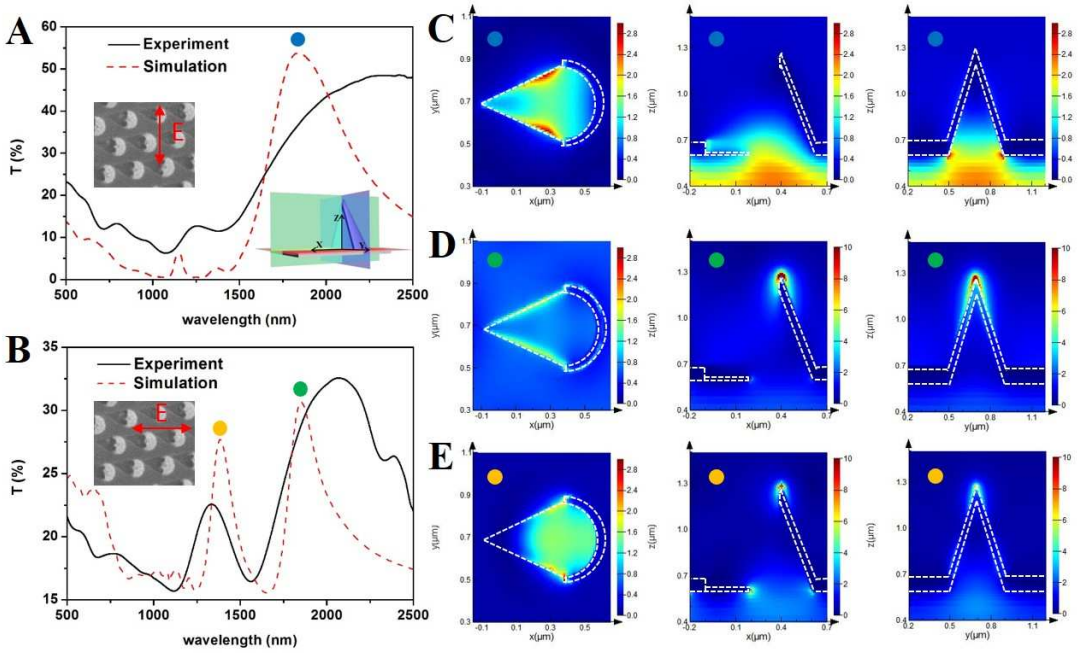

Figure 4. Experimental and simulated transmission spectra of asymmetric half-cone/nanohole arrays with 600-nm tip height for the electric field along (A) the y (short) axis and (B) the x (long) axis. The inset images show the orientation of the electric field. Simulated distributions of total normalized electric field intensity $|E|/|E_0|$ at the peak wavelengths indicated by the (C) blue, (D) green and (E) yellow dots in (A, B). The simulated planes for the graphs (C-E) are indicated in the bottom inset image in (A), which are x-y (red plane), x-z (green plane) and y-z (purple plane) from left to right, respectively. In particular, the x-y plane is at the upper side of the nanoholes (Ag/air interface). The positions of the structure are indicated by the white dotted lines in (C-E).

simulation results are in qualitative agreement with the experimental results, yet there exist some deviations of the peak position and peak width. These deviations may be caused by the structure used in the simulations not being perfectly the same as the real structure: the rough surface is not considered here; the tip may be not as sharp as that in the simulations; the inter-hole space is not uniform. In addition, simulated spectra of the thin film emerging in the shadow with various thicknesses from 30 nm to 0 nm are the same. This proves that the thin films have little effect on the SPR performance.

Furthermore, electric field distributions are displayed for each peak for the x-y plane, x-z plane and y-z plane, 4B. This can also be found from the experimental angle-dependent transmission spectra of Figure 6A, where the transmission peak position at 2070 nm does not change with the change of incidence angle. This conforms to the fact that the LSPR can hardly be affected by the incidence angle. However, for the peak at 1333 nm, the SPP due to the interaction of light with the grating remains the main element dominating the enhanced transmission. The peak is assigned as a (1, 0) Ag/glass transmission peak. LSPR can also be excited on the tip (Figure 4E) but becomes a secondary element. The explanations are supported by the simulated transmission spectra of the bottom nanohole array and top half-cone shell

array which are artificially separated from the asymmetric half-cone/nanohole array (Figure S2). The peak at 1333 nm is mainly caused by the bottom nanohole array where the coaction of SPP along the film and the LSPR around the nanoholes dominates the spectral signature,[47] and this peak corresponds to the secondary peak in Figure 4B. The half-cone shell possessing the strong LSPR on the tip is responsible for the peak at the longer wavelength. Furthermore, the peak position at 1333 nm in Figure 6A changes its position with the change of the incidence angle, which is in accord with the fact that the SPP is strongly affected by the incidence angle. Therefore, the peak at 1333 nm is mainly caused by the bottom nanohole array, yet also in combination with the LSPR at the tip. In summary, different SP modes and excited locations determined by the unique nanostructures are responsible for the strong polarization dependence, when the electric fields are along the short (y) and long (x) axis.

3.3 Spectral Dependence on Structural Parameters with Strong Polarization

Transmission spectra of the asymmetric half-cone/nanohole arrays with various heights and diameters show different spectral dependences on structural parameters for the two orthogonal polarizations (Figure 5). When the electric field is along the long axis, the main transmission peak shows a blue-shift of 381 nm by changing the height from 600 nm to 300 nm (Figure 5A), while for polarization along the short axis in Figure 5B the transmission peak shows a much larger blue-shift of 1056 nm (Figure 5C). The value measured for polarization along the short axis (red line) is about triple than that along the long axis (black line).

The structural dependence with strong polarization can be ascribed to the dominant elements of the peaks. The slightly decreasing hole diameter has little influence on the peak position but mainly determines the reduction of transmission intensity, which is in accord with previous reports.[48,49] Then the shift of the peak position is mainly affected by the height of the half-cone shells. In Figure 5A, the main transmission peak is caused by the LSPR excited on the tip according to the analysis above. There is little effect on the electric field at the tip by changing the height, leading to the small blue-shift, while for the peak in Figure 5B, the LSPR concentrated on the hole edge and Ag/glass interface is the dominant contribution. This LSPR is generated by the interaction of SP energy excited by the bottom hole edge and the top tip. This interaction would get much stronger by decreasing the height causing a larger blue-shift. Based on the structural dependence in optical transmission with strong polarization, the optical transmission can be tuned flexibly, which will not only make the asymmetric nanohole arrays fit versatile applications but also offer great potential for novel applications.

3.4 Asymmetric Angle-Dependent Optical Performance

Angle-dependent transmission spectra of the asymmetric half-cone/nanohole arrays are shown in Figure 6 for the orthogonal polarizations. The incident light is changed from the empty side (α) to the side of the half-cone shell (-α) for both Figure 6A and B, which is indicated by the inset schematics. The transmission intensity decreases gradually going from 40° to -40° for an electric field orientation along the long axis (Figure 6A). Furthermore, the transmission peak at about 1500 nm changes to a dip as the angle decreases. The difference amounts up to 40% at the optimized wavelength. These results present an asymmetric angle-dependent optical transmission. When the electric field orientation is along the short axis, yet with the same incident plane to that in Figure 6A, the transmission at an incidence angle from 0° to 40° and from 0° to -40° both experience a decreasing trend, which is considered to be an almost symmetric performance related to the asymmetric angle-dependent transmission in Figure 6A. This result is similar to the symmetric performance of conventional 2D nanohole arrays.[1]

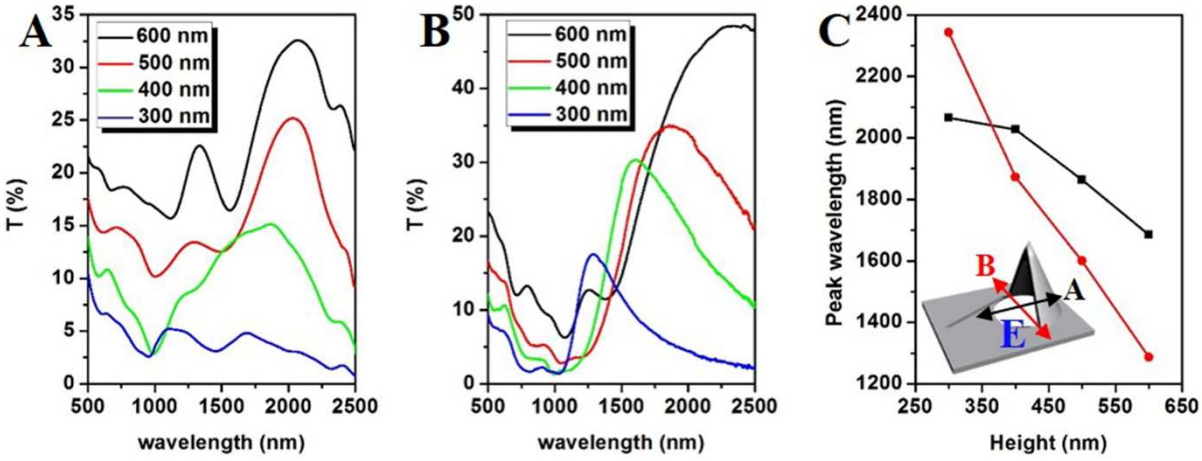

Figure 5. Transmission spectra of the asymmetric half-cone/nanohole arrays with decreasing height for the electric field being along (A) long (x) axis and (B) short (y) axis, which are indicated by the black and red arrows in (C), respectively. (C) Peak shifts for the asymmetric half-cone/nanohole arrays as a function of height. The black and red curves correspond to the results in (A) and (B), respectively.

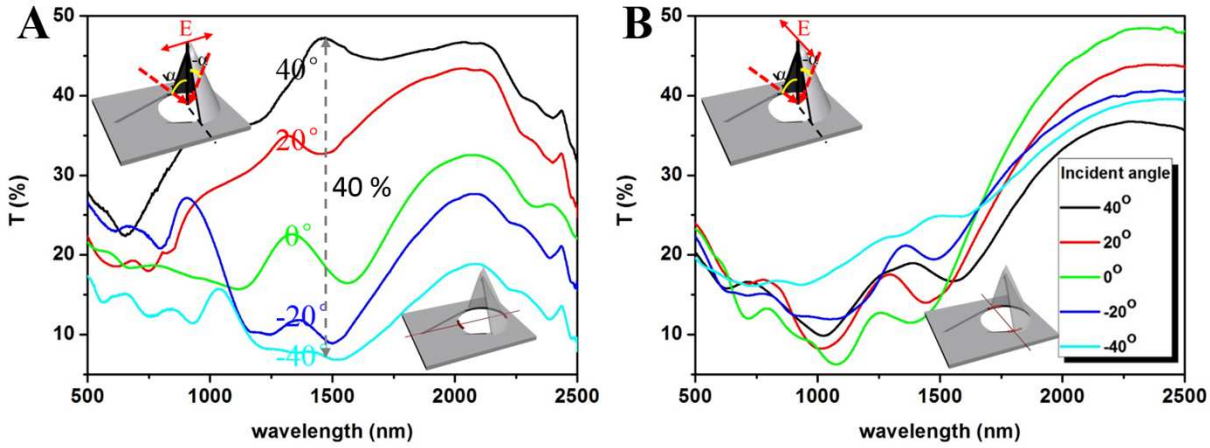

Figure 6. Transmission spectra of the asymmetric half-cone/nanohole array with 600-nm tip height for different incidence angles and for the electric field along the (A) long and (B) short axis. The top left inset schematics denote the polarizations and directions of the incident light. The bottom right inset schematics indicate the resonant positions. The maximum variation of the transmission intensity with incidence angle is 40% in (A).

The obvious differences between Figure 6A and B indicate that the asymmetric angle-dependent transmission is not induced by the directly transmitted light. This is because if the blocking function for the directly transmitted light would be the main reason, the optical performance would be the same for the two polarized light beams in Figure 6A and B, which is inconsistent with the experimental results. Actually, the nanohole arrays allow incident light to couple to a surface plasmon (SP) on one side of the film, with evanescent transfer of light through the nanoholes, and subsequent decoupling on the other side of the film. This mechanism results in the multiple optical resonance peaks. We consider that the SPR process, instead of the blocking function for the directly transmitted light, is the intrinsic factor for the optical performance of the nanohole arrays in this work. Different dominant elements of the SPR can account for the anomalous asymmetric angle-dependent transmission spectra. In Figure 6A, the transmission peak at 1333 nm is caused by the coaction of SPP along the film and the LSPR concentrated on the ends of the long asix of the nanoholes (the bottom inset image), where the SPP is strongly affected by the direction of the incident light. Moreover in this nanostructure, the half-cone shells play a significant role by providing the blocking function for the light interacting with the hot points, but with little effect on the directly transmitted light. When the light is incident from the empty side (α), more light would couple with the nanohole than if light is incident from the opposite side (-α). Then the intensity of the SPR around the hole would be more enhanced

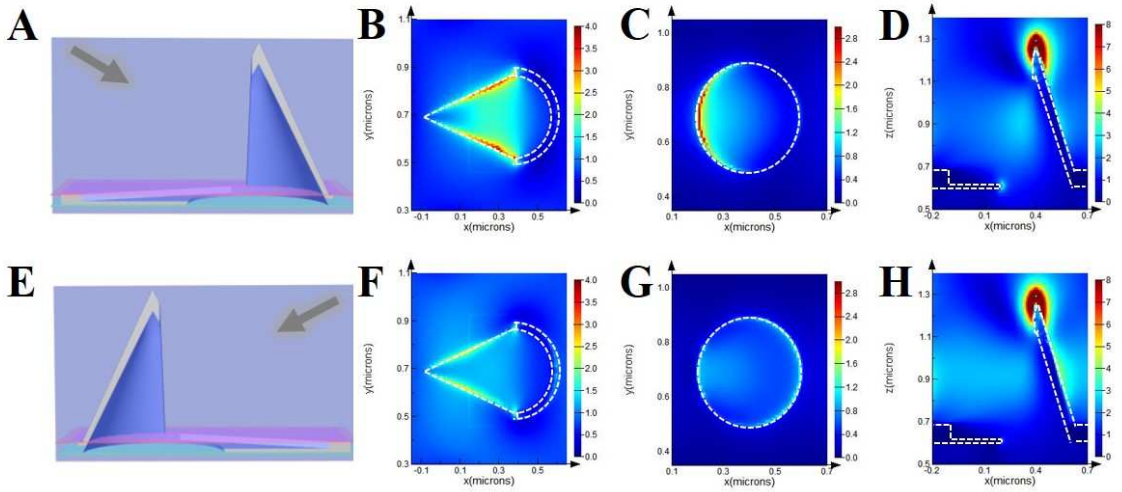

Figure 7. (A, E) Schematic displaying the direction of the incident light and the simulated planes. (B-D) and (F-H) are the simulated distributions of total normalized electric field intensity $|E|/|E_0|$ based on the conditions shown in (A) and (E), respectively. These simulations are performed for the wavelength of 1200 nm. The simulated planes are shown in (A-E), which are the (B, F) upper side of the hole (Ag/air interface, the red planes), (C, G) the bottom side of the hole (Ag/glass interface, the green planes) and (D, H) x-z (purple) planes, respectively. The positions of the structure are indicated by the white dotted lines in (B-D) and (F-H).

under the former condition and stronger optical tunneling would happen. The hypothesis above is confirmed by the simulated distributions of SP energy in Figure 7. Comparing the SP energy in Figure 7(B-D) with that in Figure 7(F-H), more effective SPs are excited when the incident light is not blocked. In particular the SP energy on the outer surface of the half-cone for conditions in Figure 7H is stronger than those in Figure 7D. This indicates that more light would be reflected back to the incident direction when the light is incident from the shelter side, which also well supports the explanations. Overall on basis of the unique SPR process, the transmission intensity presents a decreasing trend as the incident light changes from the empty side to the side of half-cone shells. Besides, the differences of the transmission intensity between the two asymmetric sides become smaller due to the weaker blocking effect as the height of the half-cone shell decreases (Figure S3). This can explain the fact that 3D crescent-like holes fabricated in previous work show only small transmission changes because of the small height.[34] The main peak in Figure 6B is caused by the LSPR concentrated on both ends of the short axis of the bottom nanohole array, as shown in the bottom inset image in Figure 4C. The light coupled with the two positions is independent from a change in incident angle. In other words, the nanoshells show no blocking function for the light interacting with the hot points. Furthermore according to previous work, the LSPR can be hardly affected by light incident from different angles.[34,50] Therefore, a small influence on the optical transmission is observed. The transmission at long wavelength (>~1650 nm) is determined by the LSPR on the film, whose light propagation distance is shorter for vertical incidence than that for inclined incident light, leading to the strongest transmission for vertical incidence. If the transmission at the wavelength <1650 nm is mainly determined by the LSPR on the inclined nanoshells, the light propagation distance of the inclined nanoshells for the incident light with angles is shorter. This is which is responsible for the weak transmission for the vertical incidence.

3.5 Preliminary Applications Based on the 3D Asymmetry

The transmission intensity of the asymmetric half-cone/nanohole array films shows sensitive responses to the incident angles, moreover possessing an asymmetric angle-dependent optical performance with respect to 180° due to the 3D asymmetry. This is more advantageous for angle-dependent sensors compared with planar (2D) asymmetric nanostructures with a cycle of 90° in transmission vs incidence angle. Figure 8A shows the transmission spectra with more incidence angles. As the incidence angle changes from 40° to 0° and continues changing to the opposite side (-40°), the transmission shows an obviously decreasing trend. The relationship between the transmission intensity and the incident angle can be analysed quantitatively, as shown in Figure 8B. The sample can recognize the incidence angle in a cycle of 180° only if the transmission is measured, which can be concluded from the curve in Figure 8B. One also can obtain a desired transmission intensity for a large range by changing the incidence angle according to the curve. This would be very useful in measuring the incident angle or changing the intensity for certain light source.

Furthermore the asymmetric angle-dependent optical performance can also be seen macroscopically without polarization (Figure 9). The results are in accord with the spectra and their explanations. The schematic of characteristic details and the optical image of the sample used are shown in Figure 9A. When the sample is illuminated from the shelter side, there are two weak dots below the sample and in the light propagation path, respectively (Figure 9B). In this case, as the inset image indicates, most of the incident light is reflected back by the shelter, which is confirmed by the fact that a bright surface is observed from the direction of incident light (Figure S4A). Therefore, only little light resulting from diffraction can couple with the hole and a weak SP is excited, leading to the weak optical transmission. Besides, the diffraction also generates the weak light dot below the sample. However compared with the light dots in Figure 9B, much brighter light dots emerge when the laser illuminates from the empty side in Figure 9C. As the inset image indicates, the incident light is reflected into the hole by the inner surface of the half-cone to excite the SP more effectively than in Figure 9B. Also the reflection directly results in the light dot below the sample. Hence there will be less light reflected back to the incident direction, which is also confirmed by the fact that a dark surface is observed from the direction of incident light (Figure S4B). Without polarized light, the nanostructure also shows asymmetric angle-dependent transmission. Natural light which

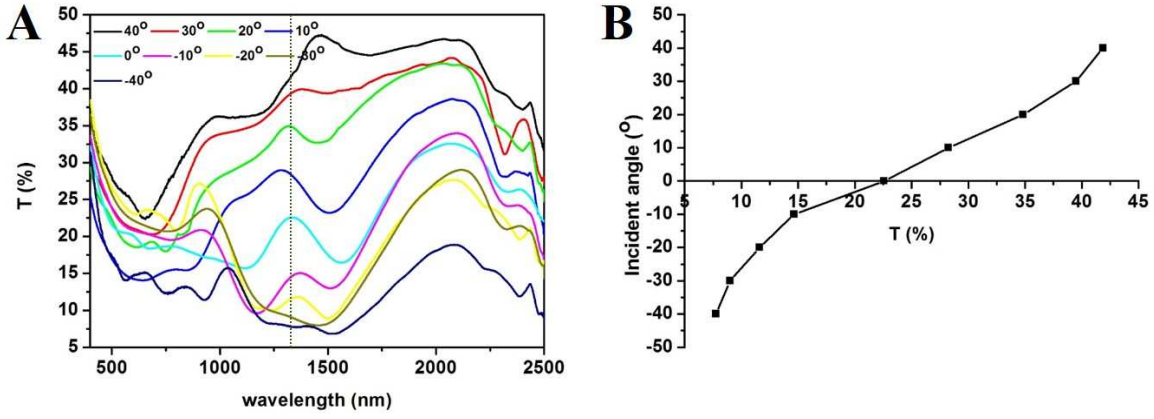

Figure 8. (A) Transmission spectra of the asymmetric half-cone/nanohole array for different incidence angles and for the electric field along the long axis as shown in Figure 6A. (B) Transmission at the wavelength 1334 nm (indicated by the dotted line in A) vs incident angle.

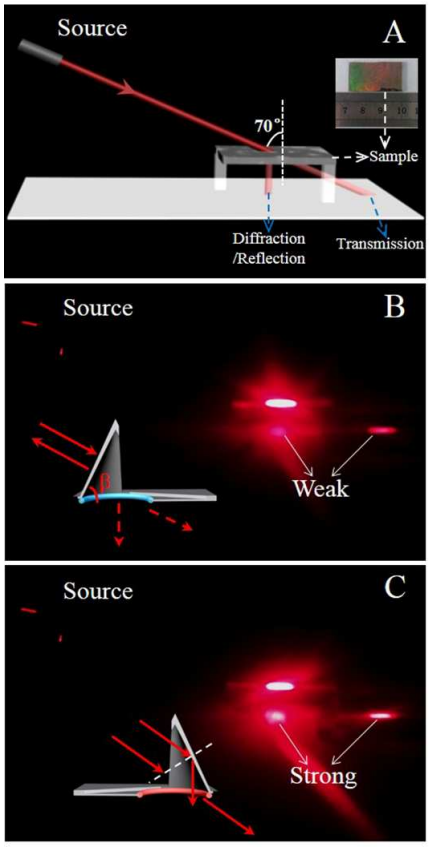

Figure 9. (A) A schematic of the characteristic details in (B) and (C). The sample supported by the two transparent pillars is illuminated by a red laser (~650 nm) with an incident angle of 70°. This procedure is carried out in dark. A white paper is placed below the sample. The inset image is an optical image of the sample. Optical images of the sample illuminated from the (B) shelter (half-cone) side and (C) empty side. The characteristic details correspond to those in (A). The angle β is about 72°. The brightest light spot is the domain illuminated by the laser on the sample.

doesn't need to be polarized can be directly used in applications to simplify the process. The property can be used in photolithography for complex patterns (gradient structures) by changing the light intensity based on the incidence angles. Besides, the asymmetric half-cone/nanohole array films can also be used for optical switches. As shown in the Video 1 in supporting information, when the incidence angle is fixed, the surface of the sample would experience a fast switch between bright and dark by rotating the sample. This suggests potential applications in ultra-fast optical switching devices.

Overall, asymmetric half-cone/nanohole arrays show the novel optical property of asymmetric angle-dependent transmission with one changing trend, which is due to the unique structural feature that the 3D asymmetric arrays possess one more degree of asymmetry than the 2D ones. The unique property offers great potential in optical switching, angle-dependent sensors and related novel optics.

4 Conclusions

In summary, a novel kind of nanohole array films is fabricated by a simple and efficient colloidal lithography method. The method is versatile, inexpensive and can be applied with only little sophisticated equipment. The nanostructured film shows a unique ability of reshaping the optical transmission based on the different heights and incidence angles with strong polarization, which is generated by different SPR modes and locations based on the 3D asymmetric nanostructure. The angle-dependent transmission of the asymmetric half-cone/nanohole arrays is asymmetric, which has strong dependence on the special 3D asymmetric feature. This is a novel property relative to the symmetric performance of the films with full-cone and 2D nanohole arrays. The films with periodic arrays of asymmetric half-cone/nanohole are believed to offer great potential for optical sensing and switching. We have concentrated here on their optical properties, but should mention that they also provide excellent asymmetric substrates for anisotropic wettability, selective detection and related potential uses. Besides the practical applications, the analysis based on the novel nanostructures yields detailed information on the interplay between the different modes and provides tuning of the local electric fields needed for sophisticated applications. In special these findings provide a novel SPR model with exciting optical performance and a means of tailoring the polarization selectivity in nanophotonic devices utilizing the SP mechanism, but also will lead to a better understanding of the physics of the SP mediated transmission.

Acknowledgements

This work was supported by the National Natural Science Foundation of China (51073070, 51173068, 51373066).

Notes and references

[a] State Key Lab of Supramolecular Structure and Materials, College of Chemistry, Jilin University, Changchun, P.R. China.
[b] Max Planck Institute of Colloids and Interfaces, Potsdam, Germany.

† Electronic Supplementary Information (ESI) available: details of the nanostructure, spectra of nanoshell arrays and nanohole arrays, angle-dependent spectra of the sample with different height, optical images of the sample. See DOI: 10.1039/b000000x/

1 T. W. Ebbesen, H. J. Lezec, H. F. Ghaemi, T. Thio and P. A. Wolff, *Nature*, 1998, **391**, 667.
2 J. R. DiMaio and J. Ballato, *Opt. Express*, 2006, *14*, 2380.
3 I. I. Smolyaninov, J. Elliott, A. V. Zayats and C. C. Davis, *Phys. Rev. Lett.*, 2005, **94**, 057401.
4 L. L. Yin, V. K. Vlasko-Vlasov, J. Pearson, J. M. Hiller, J. Hua, U. Welp, D. E. Brown and C. W. Kimball, *Nano Lett.*, 2005, **5**, 1399.
5 A. G. Brolo, S. C. Kwok, M. G. Moffitt, R. Gordon, J. Riordon and K. L. Kavanagh, *J. Am. Chem. Soc.*, 2005, **127**, 14936.
6 D. Sinton, R. Gordon and A. G. Brolo, *Microfluid. Nanofluid.*, 2008, **4**, 107.
7 A. G. Brolo, E. Arctander, R. Gordon, B. Leathem and K. L. Kavanagh, *Nano Lett.*, 2004, **4**, 2015.
8 H. F. Ghaemi, T. Thio, D. E. Grupp, T. W. Ebbesen and H. J. Lezec, *Phys. Rev. B*, 1998, **58**, 6779.
9 L. Martín-Moreno, F. J. García-Vidal, H. J. Lezec, K. M. Pellerin, T. Thio, J. B. Pendry and T. W. Ebbesen, *Phys. Rev. Lett.*, 2001, **86**, 1114.

10 F. Przybilla, A. Degiron, J. Y. Laluet, C. Genet and T. W. Ebbesen, *J. Opt. A: Pure Appl. Opt.*, 2006, **8**, 458.
11 S. G. Rodrigo, F. J. García-Vidal and L. Martín-Moreno, *Phys. Rev. B*, 2008, **77**, 075401.
12 K. Ishihara, T. Ikari, H. Minamide, J. Shikata, K. Ohashi, H. Yokoyama and H. Ito, *J. Appl. Phys.*, 2005, **44**, L929.
13 F. Miyamaru, M. Tanaka and M. Hangyo, *Phys. Rev. B*, 2006, **74**, 153416.
14 K. L. van der Molen, F. B. Segerink, N. F. van Hulst and L. Kuipers, *Appl. Phys. Lett.*, 2004, **85**, 4316.
15 K. J. K. Koerkamp, S. Enoch, F. B. Segerink, N. F. van Hulst and L. Kuipers, *Phys. Rev. Lett.*, 2004, **92**, 183901.
16 J. Elliott, I. I. Smolyaninov, N. I. Zheludev and A. V. Zayats, *Opt. Lett.*, 2004, **29**, 1414.
17 F. Miyamaru, T. Kondo, T. Nagashima and M. Hangyo, *Appl. Phys. Lett.*, 2003, **82**, 2568.
18 X. Ren, G. Guo, P. Zhang, Y. Huang, Z. Wang and G. Guo, *Appl. Phys. B: Lasers Opt.*, 2007, **89**, 257.
19 E. Altewischer, M. P. van Exter and J. P. Woerdman, *J. Opt. Soc. Am. B*, 2003, **20**, 1927.
20 T. Thio, H. F. Ghaemi, H. J. Lezec, P. A. Wolff and T. W. Ebbesen, *J. Opt. Soc. Am. B*, 1999, **16**, 1743.
21 F. Miyamaru and M. Hangyo, *Appl. Phys. Lett.*, 2004, **84**, 2742.
22 J. Henzie, M. Lee and T. Odom, *Nat. Nanotechnol.*, 2007, **2**, 549.
23 F. Przybilla, A. Degiron, C. Genet, T. W. Ebbesen, F. de Leon-Perez, J. Bravo-Abad, F. J. García-Vidal and L. Martín-Moreno, *Opt. Express*, 2008, **16**, 9571.
24 M. E. Stewart, N. H. Mack, V. Malyarchuk, J. A. N. T. Soares, T. W. Lee, S. K. Gray, R. G. Nuzzo and J. A. Rogers, *Proc. Natl Acad. Sci.*, 2006, **103**, 17143.
25 K. Nakamoto, R. Kurita, O. Niwa, T. Fujiicd and M. Nishida, *Nanoscale*, 2011, **3**, 5067.
26 J. Li, S. Chen, Y. Chou, M. Wu, C. H. Hsueh and W. Su, *J. Phys. Chem. C*, 2011, **115**, 24045.
27 S. Y. Lee, S. H. Kim, S. G. Jang, C. J. Heo, J. W. Shim and S. M. Yang, *Anal. Chem.*, 2011, **83**, 9174.
28 H. Im, S. H. Lee, N. J. Wittenberg, T. W. Johnson, N. C. Lindquist, P. Nagpal, D. J. Norris and S. H. Oh, *ACS Nano*, 2011, **5**, 6244.
29 H. Chen, L. Pang, A. Kher and Y. Fainman, *Appl. Phys. Lett.*, 2009, **94**, 073117.
30 B. Ai, Y. Yu, H. Möhwald and G. Zhang, *Nanotechnology*, 2013, **24**, 035303.
31 B. Ai, Y. Yu, H. Möhwald and G. Zhang, *Adv. Opt. Mater.*, 2013, **1**, 724.
32 B. Ai, Y. Yu, H. Möhwald, L. Wang and G. Zhang, *ACS Nano*, 2014, **8**, 1566.
33 B. Ai, Y. Yu, H. Möhwald, G. Zhang and B. Yang, *Adv. Colloid Interface Sci.*, 2014, **206**, 5.
34 Y. Shen, M. Liu, J. Li, X. Chen, H. Xu, Q. Zhu, X. Wang and C. Jin, *Plasmonics*, 2012, **7**, 221.
35 E. Altewischer, C. Genet, M. P. van Exter, J. P. Woerdman, P. F. A. Alkemade, A. van Zuuk and E. W. J. M. van der Drift, *Opt. Lett.*, 2005, **30**, 90.
36 T. Ohno, J. A. Bain and T. E. Schlesinger, *J. Appl. Phys.*, 2007, **101**, 083107.
37 B. Brian, B. Sepulveda, Y. Alaverdyan, L. M. Lechuga and M. Kaell, *Opt. Express*, 2009, **17**, 2015.
38 J. S. Shumaker-Parry, H. Rochholz and M. Kreiter, *Adv. Mater.*, 2005, **17**, 2131.
39 F. Q. Zhu, D. Fan, X. Zhu, J. G. Zhu, R. C. Cammarata and C. L. Chien, *Adv. Mater.*, 2004, **16**, 2155.
40 R. Bukasov and J. S. Shumaker-Parry, *Nano Lett.*, 2007, **7**, 1113.
41 H. Fredriksson, Y. Alaverdyan, A. Dmitriev, C. Langhammer, D. S. Sutherland, M. Zaech and B. Kasemo, *Adv. Mater.*, 2007, **19**, 4297.
42 J. Prikulis, P. Hanarp, L. Olofsson, D. Sutherland and M. Kall, *Nano Lett.*, 2004, **4**, 1003.
43 G. Zhang and D. Wang, *J. Am. Chem. Soc.*, 2008, **130**, 5616.
44 G. Zhang, D. Wang and H. Möhwald, *Nano Lett.*, 2007, **7**, 3410.
45 G. Zhang and D. Wang, *Chem.-Asian J.*, 2009, **4**, 236.
46 J. Rybczynski, U. Ebels and M. Giersig, *Colloids Surf. A*, 2003, **219**, 1.
47 S. H. Lee, K. C. Bantz, N. C. Lindquist, S. H. Oh and C. L. Haynes, *Langmuir*, 2009, **25**, 13685.
48 A. Naweed, F. Baumann, W. A. Bailey, A. S. Karakashian and W. D. Goodhue, *J. Opt. Soc. Am. B*, 2003, **20**, 2534.
49 E. Laux, C. Genet and T. W. Ebbesen, *Opt. Express*, 2009, **17**, 6920.
50 S. G. Rodrigo, O. Mahboub, A. Degiron, C. Genet, F. J. García-Vidal, L. Martín-Moreno and T. W. Ebbesen, *Opt. Express*, 2010, **18**, 23691.